MESOMECHANICAL MODELING OF CONCRETE SHOCK RESPONSE EXPERIMENTS AND LINKING TO MACROMECHANICS BY NUMERICAL ANALYSIS

Klaus Thoma*, Werner Riedel, Stefan Hiermaier

Fraunhofer Institut für Kurzzeitdynamik, Ernst-Mach-Institut (EMI)
Eckerstraße 4, D-79106 Freiburg, email: Thoma@emi.fhg.de

Key words: Hydrocodes, Material, Concrete, Shock, mesomechanical, micromechanical

Abstract: *Wherever dynamic loading conditions are of interest within the computational design and assessment of structures, material models are needed to describe the complex strength and failure behaviour of the involved materials. The less continuous and homogeneous a material is, the more complex becomes the mathematical description of its dynamic behaviour. This document describes the link of dynamic concrete models on two different geometrical scales. Parameters for describing macroscopic stress wave propagation are derived from mesomechanical (direct) simulations of the discontinuous composite of aggregate, mortar and pores. The numerical tool 'hydrocode' is described and used for computationally linking the components properties to the composite behaviour. This allows the replacement of a larger number of complex experiments with important scattering by a reduced set of standard tests together with simulations. The approach is quantitatively verified for linear (acoustic) component properties. Then the complexity is increased to non-linearity, porous compaction, plasticity and shock wave behaviour. Thus, a new mixed experimental-numerical methodology for deriving Hugoniot data for concrete and other multiphase materials is established and demonstrated for two current concrete mixtures.*

1. Introduction

The macroscopic strength and failure behaviour of concrete under quasistatic multi-axial loading has been widely studied with respect to civil engineering applications and has led to sophisticated models for numerical simulations (see Chen [1]). Loading events dominated by high frequency stress waves, however, demand a more detailed description of the dynamic behaviour. For these type of applications, numerical tools of the class 'hydrocodes' have been successfully employed during the last decades. They describe non-linear response to shock loading by solving the conservation equations for mass, momentum and energy (see next chapter). An additional relationship between pressure, volume and energy from an 'equation of state' specific to the material provides a solvable set describing the purely hydrodynamic portions of stresses and strains.

The extension to solid behaviour is achieved by including deviatoric strength. For concrete, most models use the static strength properties with strain rate dependent enhancement factors. Descriptions of damage and post-failure response give the possibility to apply hydrocodes to impact and blast loading applications with extremely high deformations, damage, failure and residual friction resistance. This approach proved to be practical (e.g. Holmquist et al. [2], Riedel [3], Gebbeken, Ruppert [4]).

Problems occur during the determination of equation of state parameters for concrete. Planar impact experiments, the standard method for characterising homogeneous solid materials, suffer from the large scale heterogeneity of concrete (Grady [5],[6] and Kipp, Chhabildas [7]). As the analysis is based on the assumption of uniaxial strain during the plate impact, it can be only applied with restrictions to concrete samples. Grady reported about reverse planar impacts of scaled concrete and thus derived the concrete Hugoniot curve with reduced but still significant scattering. Some authors (e.g. Eibl, Ockert [8]) used contact detonations on much larger concrete samples. They derived parameters from arrival times at stress gauges in the concrete. Yet, this methodology suffers from deficiencies of metrology. A third methodology consists of using complex hydraulic devices for performing static compression tests on representative concrete samples under triaxial stress control (e.g. Hanchak et al. [9], Sheridan [10]). In spite of all those attempts, the correlation between input parameters for numerical simulation provided by the different experiments is still not satisfactory. The effects of internal processes like porous compaction, complex strain distributions, localisation and failure superimposed to a macromechanical shock response are only qualitatively understood.

Static 'mesomechanical' simulations by numerous authors, describing directly the concrete composite of internally homogeneous mortar and aggregate grains provided some additional insight to the above points. Amieur et al. [11] employed this methodology in order to analyse the effective 'macroscopic' properties of statically loaded heterogeneous concrete samples in comparison to analytical investigations on the bounds of elastic composites by Hill, Voit and Reuss (see also chapter 5 and Hill [12]).

Kipp, Chhabildas [6] and Thoma, Riedel [13] showed first extensions of 'mesomechanical simulations' to wave propagation problems in concrete. In addition to the above mentioned static effects, internal shock reverberations and scattering in the arrival times of stress waves could be reproduced in hydrocode simulations. Yet, the assumed material properties were relatively simple and no link was made to derive macromechanical equation of state properties. The present work continues the studies in this direction.

2. Hydrocodes as Tool for Dynamic Mesomechanical Modeling

With the prospect of extending the study to nonlinear shock response, a 'wave propagation code' or 'hydrocode' is used as a numerical tool. In the present study the conservation equations for mass, momentum and energy (equations 1a, b, c, Lagrangian referential, index notation) are solved together with the constitutive equations (see below) by the commercial finite difference scheme AUTODYN [14]. Here, stresses and strains are decomposed in volumetric and deviatoric portions (2).

Mass conservation:
$$\frac{D\rho}{Dt} + \rho \frac{\partial v_i}{\partial x_i} = 0 \qquad (1a)$$

Momentum conservation:
$$\rho \frac{Dv_i}{Dt} = -\frac{\partial p}{\partial x_i} + \frac{\partial S_{ji}}{\partial x_j} + \rho f_i \qquad (1b)$$

Energy conservation:
$$\rho \frac{De}{Dt} = \rho \dot{q} + \frac{\partial}{\partial x_i}\left(k \frac{\partial T}{\partial x_i}\right) - p \frac{\partial v_i}{\partial x_i} + S_{ji} \frac{\partial v_i}{\partial x_j} \qquad (1c)$$

Decomposition of stresses:
$$\boldsymbol{s}_{ab} = S_{ab} - p\boldsymbol{d}_{ab} \qquad (2)$$

With S_{ij} set to zero in (1a-c), one describes a fluid without shearing resistance. In this case an 'equation of state' (referred to as 'EOS' below) linking pressure, density and internal energy (3) provides a solvable set of equations.

$$p = p(\rho, e) \quad \text{e.g. ideal gas} \qquad (3)$$

Describing strength of solid materials, the 'Jaumann' tensor of stress rates is used as objective measure for deviatoric stresses S_{ij}. Thus, Hook's law is given in (4).

$$\dot{S}_{ij} = \underbrace{S_{ij}\dot{R}_{jk} + S_{kj}\dot{R}_{ik}}_{\text{rotation correction}} + G\left(\dot{\varepsilon}_{ij} - \tfrac{1}{3}\delta_{ij}\dot{\varepsilon}_{kk}\right) \qquad (4)$$

Coordinates, velocities and accelerations are node variables in the computational grid, while material properties such as mass, pressure, deviatoric stresses, internal energy, etc. are evaluated in the cell centre. Quadrilateral 4-node elements are used in two dimensional calculations (plain strain assumption) and 8-node brick elements for 3D discretisations. Time integration is performed by an explicit central difference scheme under time step control using the 'Courant-

Friedrich-Levy'-criterion. Thus, high frequency stress waves are resolved and rotations can be considered small per timestep (condition for equation 4).

The discontinuity of state variables across the shock front causes oscillations in the numerical solution. That is why hydrocodes employ, in general, an 'artificial viscosity' in order to smear out the shock over several cells. The term added to the hydrostatic pressure in (1b) employed in AUTODYN is given in (5). The attention shall be drawn to the fact, that only compressive waves are smeared out. Thus, oscillations in shear waves are not avoided as they do not provide a change in density.

$$q = \rho \left[\left(C_{Qad} d \left(\frac{\rho}{\dot{\rho}} \right)^2 - C_{Lin} c_L d \left(\frac{\rho}{\dot{\rho}} \right) \right) \right] \tag{5}$$

3. Characterisation and Description of Concrete Components

Improved characterisation of concrete components is necessary for quantitative mesomechanical simulations. The compression properties of mortar were derived by standard methods for homogeneous materials. The porous compaction path is derived from static compression tests (see Figure 1) with heavy lateral confinement. Thus, the samples were loaded approximately under a state of uniaxial strain on the macroscopic scale. Friction between the sample and the confinement was minimised by a thin Teflon layer and oil lubrication on all surfaces.
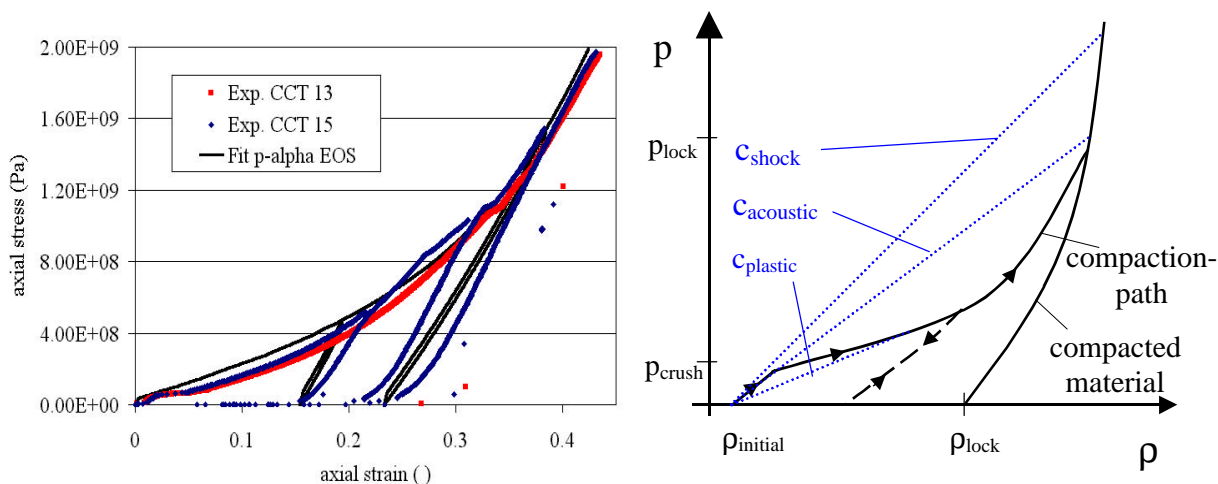

Figure 1: Porous compaction during confined compression tests and description in p-α-equation of state

Inverse planar plate experiments were used to obtain the uniaxial compression behaviour at strain rates up to 10^4/s. This method, explained in detail by Grady [6], is very well adapted to characterise the shock behaviour of unknown materials. A schematic of the test is given in Figure 2. Cylindrical mortar plates (radius 50 mm, thickness $t_{mortar} = 8$mm) covered with an Aluminium backing plate ($t_{bp} = 2$mm or 10mm) are accelerated in a gas gun to reach velocities between 150

and 1000 m/s (see Figure 3 and Table 1). The composed projectile impacts a stationary witness plate of well characterised C45-steel. Nahme [15] provided experimental data for the parameters S and c_P in equation (7) (ρ_{steel} = 7.8 g/cm³, $c_{B,steel}$ = 4480 m/s, S_{steel} = 1.332). A VISAR laser interferometer systems records the velocity trace of the witness plate during the impact with a resolution in the nanosecond range (see Figure 3).
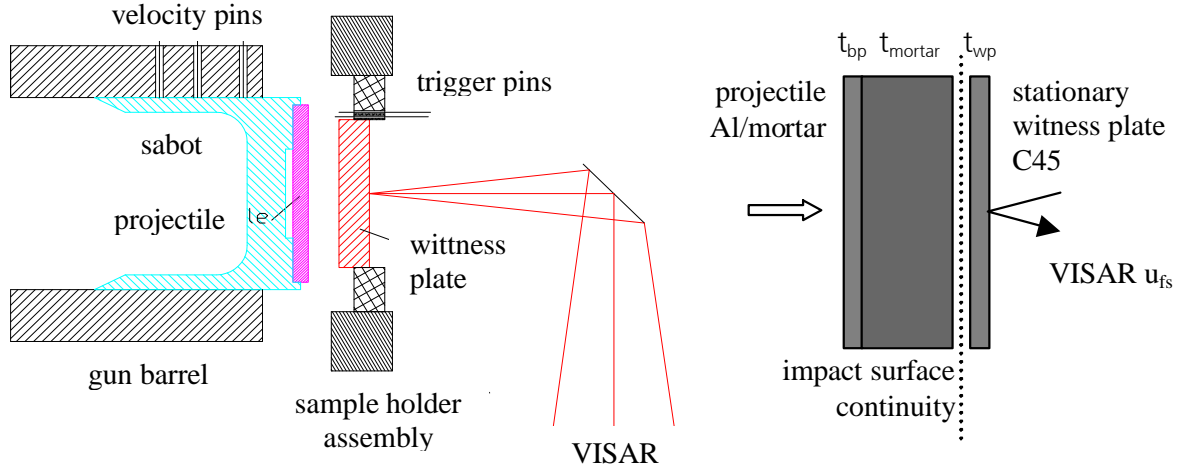

Figure 2: Configuration of inverse planar impact experiments

Continuity of pressure and particle velocity is required at the impact surface. The first jump in the free-surface velocity u_{fs} allows calculation of both variables by using the equation of state of the witness plate. Employing the Hugoniot relations (6a-c) and the known equation of state properties of the C45-steel the complete impact conditions in the mortar can be calculated through equations (8a-c) without any assumption on the mortar's equation of state.

$$\sigma_h = \rho_0 U_s u_p \quad (6a) \qquad \frac{\rho_0}{\rho} = \frac{V}{V_0} = \frac{U_s - u_p}{U_s} \quad (6b) \qquad e = \frac{1}{2}\left(\frac{1}{\rho_0} - \frac{1}{\rho}\right)\sigma_h \quad (6c)$$

$$U_s = S \times u_p + c_P \tag{7}$$

$$\sigma_h = \rho_{witness} c_{B,witness}\left(\frac{1}{2}u_{fs1}\right) + \rho_{witness} S_{witness}\left(\frac{1}{2}u_{fs1}\right)^2 \tag{8a}$$

$$u_{p,mortar} = v_{imp} - \frac{1}{2}u_{fs1} \tag{8b}$$

$$U_{s,mortar} = \frac{\sigma_h}{\rho_{0,mortar} u_{p,mortar}} \tag{8c}$$

But inverse planar impacts allow even wider analysis. After shocking the concrete projectile and the witness plate on the contact surface to their respective Hugoniot states, the stress waves travel through both plates. Release states emerging on the free surface of the witness plate result in subsequent velocity jumps (see Figure 3). A last big step is due to the reflection of the compression wave from the interface between the mortar sample and the aluminium backing.

5

Thus, the delay between the Hugoniot state and this last step is the time needed by the compressive wave to travel forward through the uncompressed and back through the compressed material. All these characteristics can be very well used as milestones for numerical simulations of uniaxial strain loading.
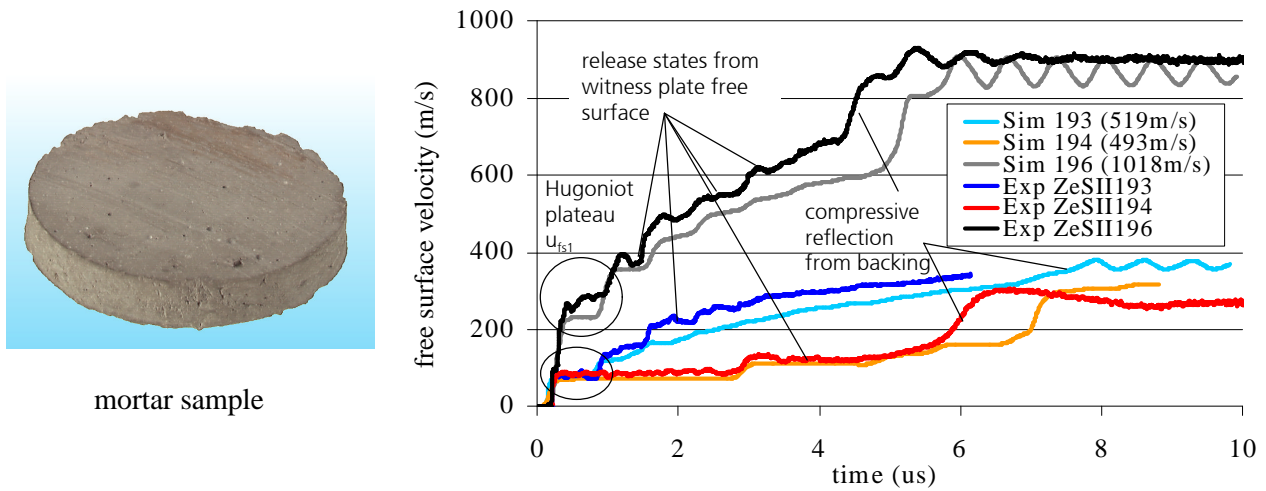

Figure 3: Experimental and simulated velocity traces

Exp. No.	$t_{witnessplate}$ (mm)	t_{mortar} (mm)	$t_{backing}$ (mm)	v_{imp} (m/s)	u_{fs1} (m/s)	u_p (m/s)	σ_h (GPa)	U_s (m/s)
ZeSII193	2	8	3.32	519	88.6	475	1.57	1543
ZeSII194	8	8	10	493	84.4	451	1.49	1547
ZeSII196	2	8	3.33	1018	280	878	5.10	2712
ZeSII197	8	8	10	948	275	810	4.93	2841
ZeSII198	2	8	3.32	742	150	667	2.68	1877
ZeSII199	8	8	10	712	142	641	2.53	1847
ZeSII200	8	8	10	960	248	836	4.49	2511

Table 1: Configurations and results of reverse planar impact tests

Figure 3 shows the simulation of three inverse planar impact experiments using the data set adapted in [13] on direct flyer plate tests on the same material. The employed porous equation of state proposed by Herrmann [16] takes into account the porous phase of the material by scaling the behaviour of the matix material over the porosity α (see equation (9) and Figure 1). All important features as the plateau provided by the initial shock conditions ('Hugoniot plateau'), subsequent release states and final velocities are well reproduced. Quantitative deviations (e.g. the arrival time of the pressure reflection from the backing plate) are moderate so that the data seems suited for application in mesomechanical simulations.

$$p = f(\rho, e) \quad \overset{porous}{\rightarrow} \quad p = f(\rho\alpha, e) \quad with \quad \alpha = 1 + (\alpha_{init} - 1)\left[\frac{p_{lock} - p}{p_{lock} - p_{crush}}\right]^n \qquad (9)$$

Unconfined compression tests and ultrasonic measurements of acoustic wave velocities characterise the elastic behaviour such as the Young's modulus and acoustic wave speeds (c_p=3840m m/s). Furthermore, the unconfined compression test provides the input for the elastic-

plastic strength model with an isotropic plastic strain failure limit. The results of all tests are combined into one consistent description for the strength behaviour ranging from elastic to permanent deformation and from quasistatic loading up to non-linear shock response under strain rates up 10^4/s. Refinement of the data and a more detailed description of the derivation will be the subject of future publications.

Dynamic properties of geomaterials have been widely studied (e.g. Marsh [17]). Considering the general scattering of mechanical rock properties, the aggregate can be reasonably described by literature data. A few self-conducted plate impact experiments on this material showed the correlation to the employed aggregate. An overview of the resulting material data set for mesomechanical simulations is given in Table 2.

Aggregate (Granite)			Mortar with sand		
Shock EOS [17]	ρ	2.679 g/cm³	p-α EOS	ρ_{porous}	2.14 g/cm³
	c_B	3750 m/s		$c_{B,porous}$	2342 m/s
	S	1.03		p_{crush}	5.0 MPa
				p_{lock}	2.5 GPa
				N	3
			Solid EOS linear	$\rho_{compacted}$	2.9 g/cm³
				K	46.40 GPa
Strength v.Mises	G	33.87 GPa	Strength v.Mises	G	11.66 GPa
	σ_Y	0.888 GPa		σ_Y	0.120 GPa
	p_{min} (spall)	-40 GPa		p_{min} (spall)	-4.0 MPa

Table 2: Employed material data

4. Describing Concrete Mixtures

For numerical simulations on the mesomechanical scale the concrete is decomposed into two 'sub-materials' (see Figure 4) which can be considered homogeneous with respect to the sample sizes in the experiments. The sub-material mortar consists of the hardened cement paste and the fraction of aggregate smaller than 1 mm in diameter. Moreover, the mortar is assumed to contain all pores of the concrete.

In order to model the concrete microstructure, a preprocessor routine randomly distributes spherical aggregate particles within the mesh initially filled with mortar material until the overall composite density is obtained. The aggregate size distribution follows the specifications for sieve-lines of the German norm DIN 1045. Figure 5 gives an example of four mass distributions with maximum grain size of 16 mm. Two different concrete densities with different grains distributions have been numerically composed for the present study (see Table 3). An important point is the fact that both mixtures consists of the same 'sub-materials', mortar and aggregate, with data as given in Table 2. The concrete mixture is specified and composed in the computer during the preprocessing.

A stress pulse is introduced as a velocity jump condition on one free surface of the concrete sample. Longitudinal ('p-') waves are excited normal and shear waves parallel to the boundary.

Within the discretised area the respective wave velocity can be calculated as the distance of the considered cell centre divided by the arrival time. Only cells with sufficient distance from the other free surfaces are taken into account in order to observe the wave propagation in an unbounded media without influences from release waves. Here, the mesh resolution is highest, gradually decreasing towards the edges.
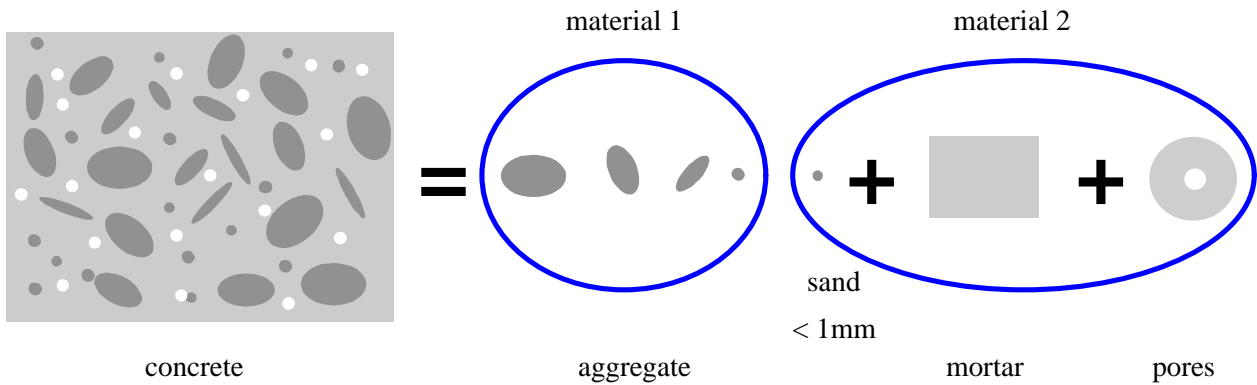

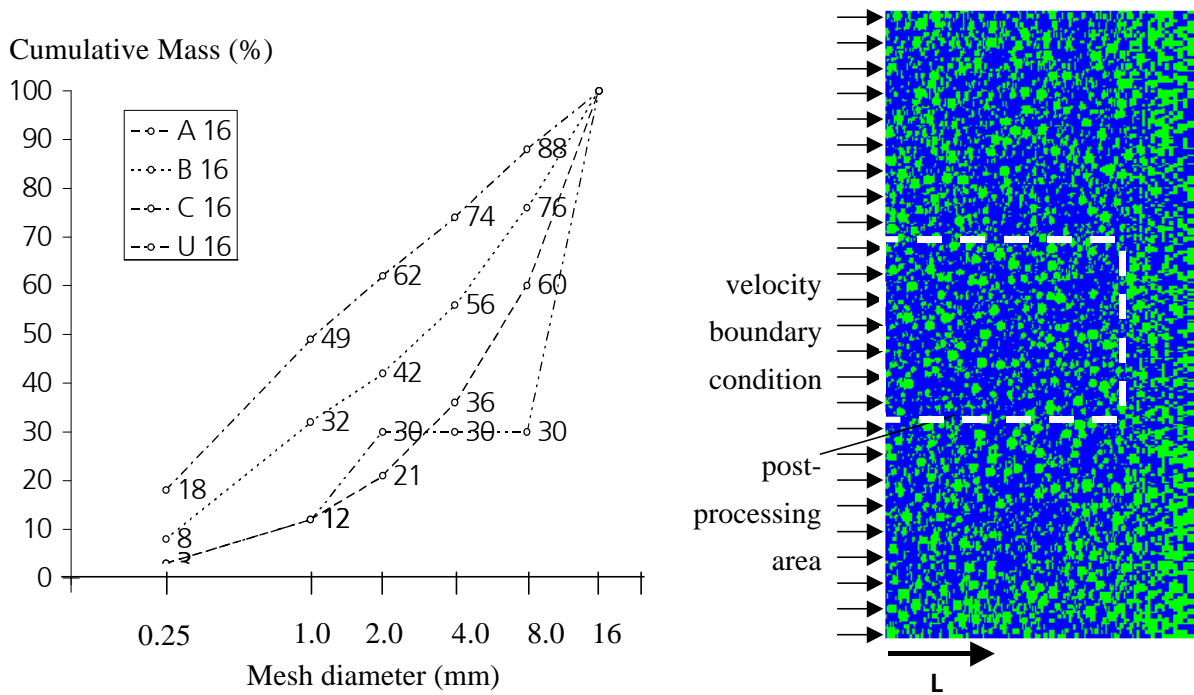Figure 4: Consideration of concrete as a mixture of two ‚homogeneous' materials

Figure 5: Concrete size distributions according to DIN 1045

Mixture	ρ_{mortar} (g/cm³)	$\rho_{aggregate}$ (g/cm³)	$\rho_{concrete}$ (g/cm³)	max. grain size (mm)	distribution DIN 1045
A	2.14	2.679	2.31	8	A 8
B	2.14	2.679	2.45	42	A 32

Table 3: Simulated concrete mixtures

A postprocessing routine checks every cell at every time step, to determine whether the local velocity has reached half of the particle velocity imposed by the boundary condition. Thus elastic, plastic and shock waves can be separated and the result is independent of viscosity smoothing (see Figure 6). The output of the postprocessor routine is the wave velocity ($t_{trigger}/L$) over the distance from the excitation L. Figure 7 shows that scattering is maximum close to L=0. Maximum and minimum values are defined by the respective material wave speeds. Over the propagation distance L, the bandwith reduces to the inherent scattering of the composite. It is defined by the differences in wave speeds and the maximum grain size. In the latest treatment, the mean value and the standard deviation are calculated from the data sets of wave velocities at the same distance L.
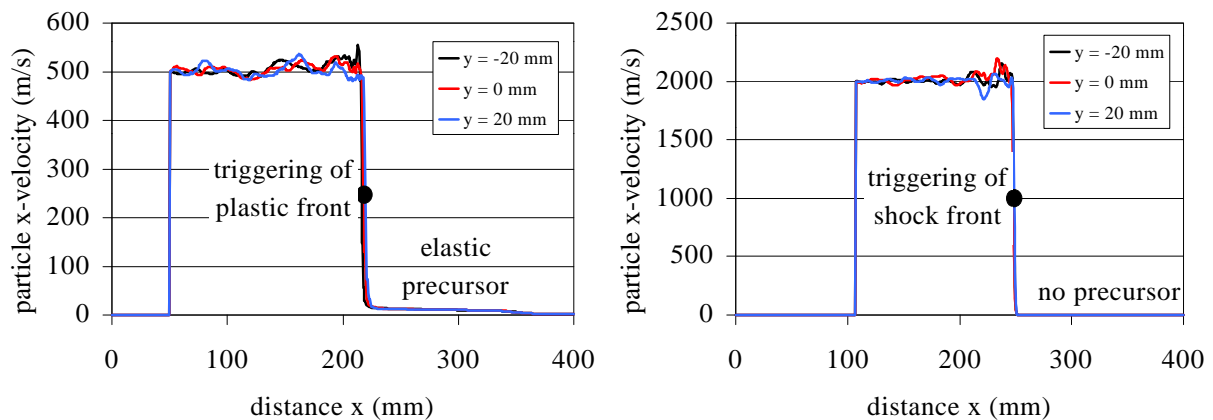
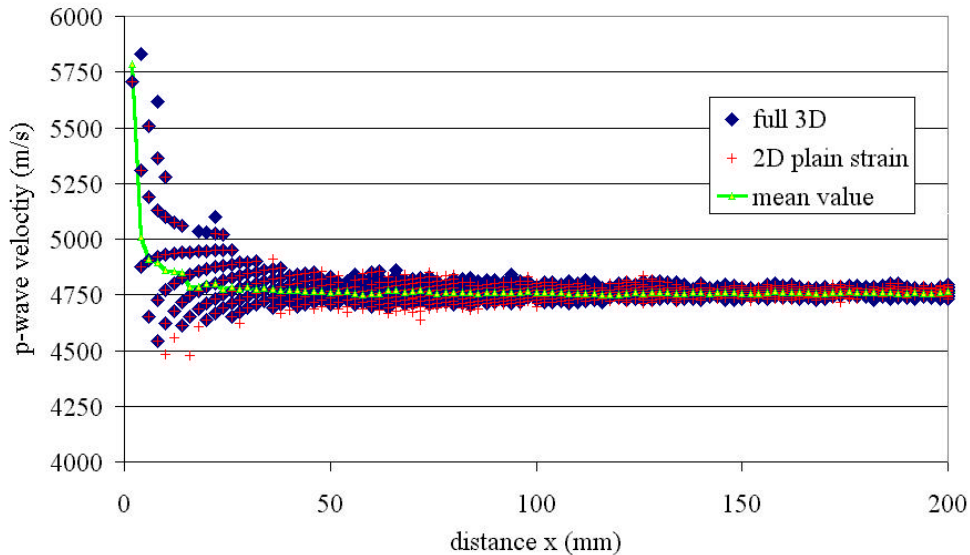Figure 6: Triggering of wave arrival times

Figure 7: Comparisons of 3D and 2D plain strain wave velocities

Both pre- and postprocessors have been implemented in 2D and 3D Lagrangian hydrocodes. Figure 7 shows the calculated wave speeds in one slice of elements in a full 3D calculation (blue squares). In order to validate 2D calculations, the distribution of the same slice was subjected to a lateral displacement constraint, thus imposing 2D plain strain conditions. The red crosses in the

9

same figure mostly overlay the 3D results and converge towards the same wave speed. Consequently, two dimensional calculations were applied in the following, allowing the use of higher grid resolutions.

5. Quantitative Linking of Meso- and Macromechnanical Models

Quantitative linking of mesomechanics and macromechanics is initially verified in the elastic-acoustic loading range. Effective properties of elastic composites have been studied by several authors. Hill [12] provided an overview on bounds of the effective elastic properties of mixtures. Voigt derived an upper bound assuming uniform stresses throughout the mixture (10). A lower limit was proposed by Reuss assuming uniform strain (11). f_i denotes in the following the volume fractions of the constituents with $f_1 + f_2 = 1$.

$$K_V = f_1 K_1 + f_2 K_2 \qquad\qquad G_V = f_1 G_1 + f_2 G_2 \qquad\qquad (10)$$

$$\frac{1}{K_R} = \frac{f_1}{K_1} + \frac{f_2}{K2} \qquad\qquad \frac{1}{G_R} = \frac{f_1}{G_1} + \frac{f_2}{G_2} \qquad\qquad (11)$$

Hashin and Shtrikman deduced closer bounds by applying variational principles on the stress-strain distributions in the composite (12a, b).

$$K_2 + \frac{(K_1 - K_2)f_1}{1 + \alpha_2 f_2 \left({K_1}/{K_2} - 1 \right)} \leq \quad K \quad \leq K_1 + \frac{(K_2 - K_1)f_2}{1 + \alpha_1 f_1 \left({K_2}/{K_1} - 1 \right)} \qquad (12a)$$

$$G_2 + \frac{(G_1 - G_2)f_1}{1 + \beta_2 f_2 \left({G_1}/{G_2} - 1 \right)} \leq \quad G \quad \leq G_1 + \frac{(G_2 - G_1)f_2}{1 + \beta_1 f_1 \left({G_2}/{G_1} - 1 \right)} \qquad (12b)$$

$$\text{with} \quad \alpha_i = \frac{K_i}{K_i + \frac{4}{3} G_i} \qquad \beta_i = \frac{2(K_i + 2G_i)}{5(K_i + \frac{4}{3} G_i)}$$

In order to make the transition to dynamic applications, the link between elastic moduli K,G and L and acoustic wave speeds c_B, c_S and c_P is used (equations 13a, b, c). Comparing effective wave speeds calculated in acoustic mesomechanical simulations, we note that the p-wave velocity (longitudinal wave in unbounded media) converges correctly into the marging of the analytical bounds.

Shear wave velocities match the coarser estimations by Reuss and Voigt, but converge only beyond the bounds defined by Hashin and Shtrikeman. The scalar viscosity, only avoiding oscillations in compressive stress waves, might be an explanation (see above). However, shock waves occur only for strong compressive loading waves under confined conditions, so that matching of the longitudinal wave speed is of primary interest.

$$K = \rho_0 c_B{}^2 \quad (13a) \qquad\qquad G = \rho_0 c_S{}^2 \quad (13b) \qquad\qquad L = K + \tfrac{4}{3} G = \rho_0 c_P{}^2 \quad (13c)$$
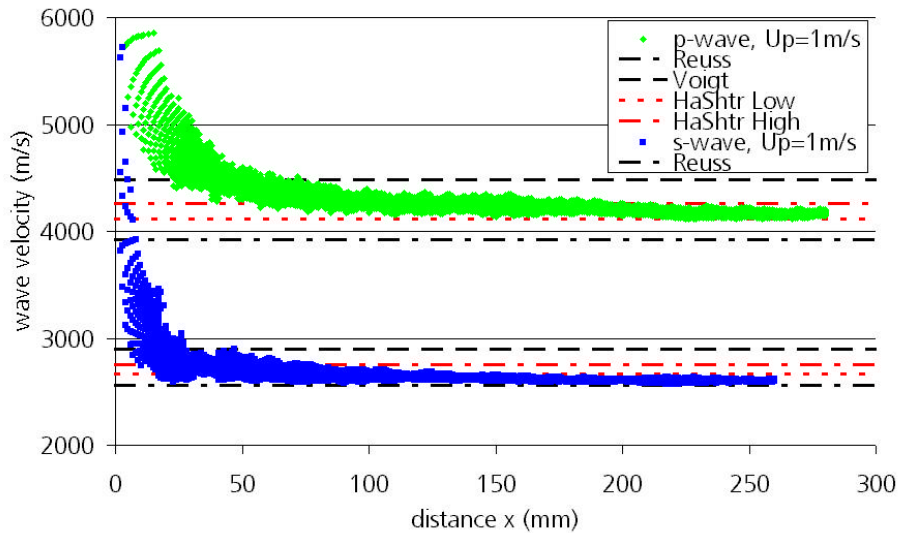
Figure 8: Comparison of simulated acoustic wave speeds to analytical bonds

After confirming the methodology for effective acoustic wave speeds, it was extended to non-linear analysis. Introducing non-linear constitutive equations for the components as described above, the shock speed in the composite can be deduced by numerical calculations. A series of calculations on identical concrete mixtures and distributions respectively was conducted by imposing particle velocities of 1, 100, 500, 1000, 1500, 2000 and 3000 m/s as boundary conditions. The results in terms of the mean shock velocity Us and its standard deviation ΔUs for mixtures A and B are given in Table 4 and compared to experimental data from literature in Figure 9. It has to be pointed out, that the experimental data of different authors was obtained for different concrete mixtures and measurement techniques. Thus, a comparison is difficult and only general trends may be observed. Moreover, all experimental tests suffer from large scattering due to the heterogeneity of the concrete samples and/or the reliability of the measurement technique.

u_p (m/s)	Mixture A $\Delta U_s \leq 45$ m/s U_s (m/s)	Mixture B $\Delta U_s \leq 150$ m/s U_s (m/s)
1	4162	4521
100	1528	1994
500	2182	2846
1000	3331	3870
1500	4066	4528
2000	4647	5052
3000	5648	6134

Table 4: Hugoniot data of concrete caculated from mesomechanical analysis

Considering the above points, a generally good correlation is observed with the literature data. The drop in p-wave velocity for particle velocities of several hundred meters per second is observed both in experiments and mesomechanical simulations. By numerical analysis, it can be clearly attributed to the decreasing slope of the compression curve during porous compaction (see Figure 1). From a minimum at u_p around 200 m/s a continued increase in wave velocity is

11

observed. A sharp shock wave without elastic precursor (see Figure 6) is observed for particle velocities exceeding 1500 m/s.
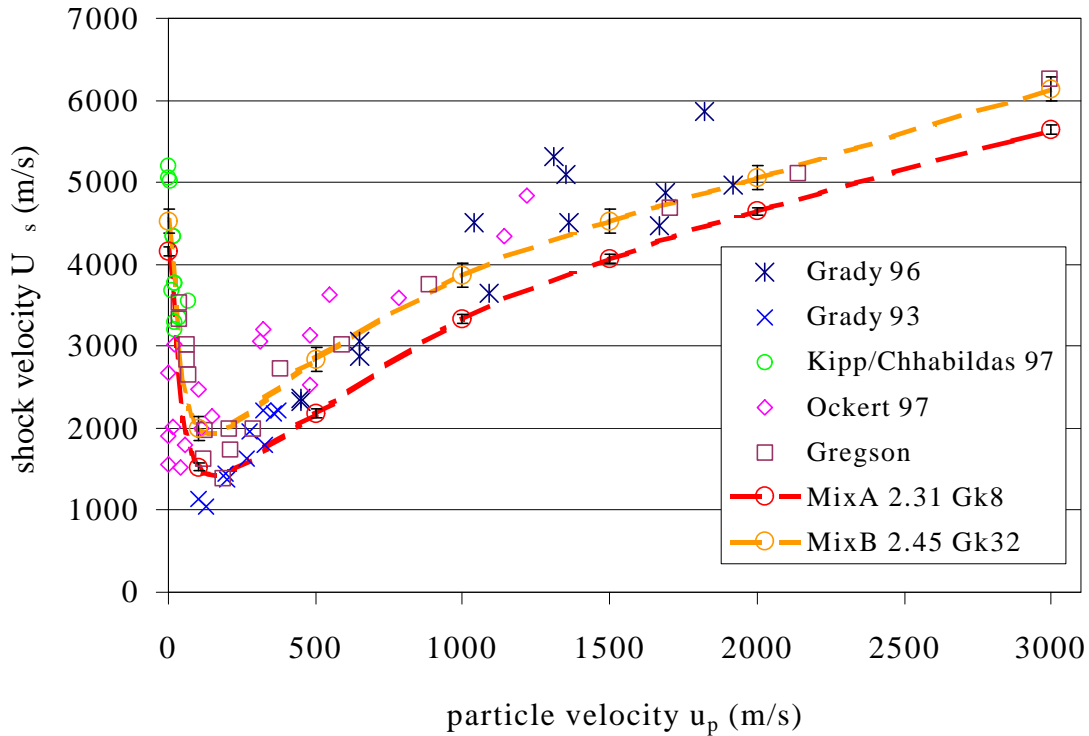

Figure 9: Comparion of mesomechanical Hugoniot data to results in literature

6. Conclusions

The introduction shortly reviews the state of the art of concrete modelling for dynamic applications. A general uncertainty about shock Hugoniot data was identified. This is due to the large scale heterogeneity of the material and subsequent experimental problems.

Nonlinear dynamic behaviour of materials under high frequency stress waves can be described by solving the conservation equations for mass momentum and energy plus constitutive laws for the considered material. Details about the discretisation in a hydrocode based on a finite difference scheme are given in chapter 2.

In the paper, concrete is explicitly modelled as a mixture of two materials which can be considered homogeneous with respect to experimental sample dimensions and numerical grid resolutions. Thus, standard techniques become applicable to determine the dynamic material properties. Special efforts were made to characterise the mortar. A combination of confined static compression tests and inverse planar impact experiments provided detailed information on the compression and compaction behaviour from static up to shock wave loading.

The methodology to derive apparent wave speeds from mesomechanical simulations is validated in the range of elastic properties. Here, quantitative comparison to analytical bounds is possible. On this basis, the study was enlarged to stronger waves including elastic-plastic loading and shock waves. The relationship between shock and particle velocity, basis of the Hugoniot curve, was derived for two current concrete mixtures.

In summary, a new mixed experimental-numerical methodology for deriving Hugoniot data for concrete and other multiphase materials has been established. It consist of a reduced set of standard experiments together with simulations in comparison to more complicated and uncertain measurement techniques employed previously.

Index

x_i	Langragian coordinate vector component
v_i	component of velocity vector
$\dfrac{D}{Dt}$	substantial derivative
p	hydrostatic pressure
ρ	density
e	internal energy
S_{ij}	component of deviatoric stress tensor
$\dot{q}$	rate of volumetric heat addition per unit mass (absorption, emission, radiation)
q	artificial viscosity term
C_{Lin}	linear constant for artificial viscosity
C_{Quad}	quadratic constant for artificial viscosity
d	characteristical cell dimension (artificial viscosity)
c_L	longitudinal soundspeed in a bar
c_b	longitudinal soundspeed in unbounded media
c_s	shear soundspeed in unbounded media
c_B	bulk soundspeed in unbounded media
K, G, L	bulk, shear an longitudinal elastic moduli
f_i	component of body force vector (gravitatinal, magnetic)
f_1, f_2	volumetric fraction of a composite constituent
k	thermal conductivity
T	temperature

References

[1] Chen W.F., Han D.J., Plasticity for Structural Engineers, ISBN 0-387-96711-7, Springer, New York, 1988

[2] Holmquist T.J., and Johnson G.R., A computational constitutive model for concrete subjected to large strains, high strain rates, and high pressures, 14th International Symposium on Ballistics, Québec, 1993

[3] Riedel W., Ein makroskopisches, modulares Betonmodell für Hydrocodes mit Verfestigung, Schädigung, Entfestigung, Drei-Invariantenabhängigkeit und Kappe, EMI report 7/98, Freiburg, 1998

[4] Gebbeken N., Ruppert M., A New Concrete Material Model for High Dynamic Hydrocode Simulations, to be published in Archive of Applied Mechanics, Universität der Bundeswehr, München, 1999, private communication

[5] Grady D.E., Impact Compression Properties of Concrete, 6th Int. Symposium on Interaction of Nonnuclear Munitions with Structures, Panama City, Floridy, May 3-7, 1993

[6] Grady D.E., Dynamic Decompression Properties of Concrete from Hugoniot States – 3 to 25 GPa, Experimental Impact Physics Departement, Technical Memorandum TMDG0396, Feb. 1996

[7] Kipp M.E., Lalit, Chhabildas C., Elastic Shock Response and Spall Strength of Concrete, proceedings of APS 1997

[8] Ockert J., Ein Stoffgesetz für die Schockwellenausbreitung in Beton, PhD thesis, Technische Hochschule Karlsruhe, 1997

[9] Hanchak S.J., Forrestal M.J., Young E.R., Ehrgott J.Q., Perforation of Concrete Slabs with 48 MPa (7 ksi) and 140 MPa (20 ksi) Unconfined Compressive Strength, Int. J. Impact Engineering, Vol. 12, No.1, pp. 1-7. 1992

[10] Sheridan A.J., Application of Concrete Triaxial Data to Hydrocodes, DRA Working Paper MTC-91-WP-26, RAE, Farnborough, Hampshire, June 1991

[11] Armieur M., Hazanov S., Huet C., Numerical and experimental study of size and boundary conditions effects on the apparent properties of specimens not having the representative volume, Micromechanics of concrete and cementitious composites, ed. C. Huet, ISBN 2-88074-260-9, Lausanne, 1993

[12] Hill R., Elastic Properties of Reinforced Solids: Some Theoretical Principles, J. Mech. Phys. Solids, Vol. 11, pp. 357-372, 1963

[13] K.Thoma, W.Riedel, H. Nahme, B.Lexow, E.Straßburger, H.Senf, Shock Wave Phenomena in Concrete - Impact Tests and Mesomechanical Simulations, Transient Loading and Response of Structures, International Symposium honouring Mr. Arnfinn Jenssen, Trondheim May 25-27, 1998

[14] AUTODYN, Theory Manual, Century Dynamics Ltd. Horsham, England, 1997

[15] Nahme H., Equation of State Measurements of 9SMn28- and C45-Steel, EMI report E11/91

[16] Herrmann W., Constitutive Equation for the Dynamic Compaction of Ductile Porous Materials, Journal of Applied Physics, Vol 40, No 6, 1969, pp. 2490-2499

[17] Marsh S.P. (Editor), LASL Shock Hugoniot Data, University of California Press, 1980